

# Rewritable three-dimensional holographic data storage via optical forces

Yetisen, Ali K.; Montelongo, Yunuen; Butt, Haider

DOI:

[10.1063/1.4960710](https://doi.org/10.1063/1.4960710)

License:

None: All rights reserved

*Document Version*

Peer reviewed version

*Citation for published version (Harvard):*

Yetisen, AK, Montelongo, Y & Butt, H 2016, 'Rewritable three-dimensional holographic data storage via optical forces', *Applied Physics Letters*, vol. 109, no. 6, 061106. <https://doi.org/10.1063/1.4960710>

[Link to publication on Research at Birmingham portal](#)

## **Publisher Rights Statement:**

The following article appeared in (citation of published article) and may be found at (URL/link for published article abstract).

## **General rights**

Unless a licence is specified above, all rights (including copyright and moral rights) in this document are retained by the authors and/or the copyright holders. The express permission of the copyright holder must be obtained for any use of this material other than for purposes permitted by law.

- Users may freely distribute the URL that is used to identify this publication.
- Users may download and/or print one copy of the publication from the University of Birmingham research portal for the purpose of private study or non-commercial research.
- User may use extracts from the document in line with the concept of 'fair dealing' under the Copyright, Designs and Patents Act 1988 (?)
- Users may not further distribute the material nor use it for the purposes of commercial gain.

Where a licence is displayed above, please note the terms and conditions of the licence govern your use of this document.

When citing, please reference the published version.

## **Take down policy**

While the University of Birmingham exercises care and attention in making items available there are rare occasions when an item has been uploaded in error or has been deemed to be commercially or otherwise sensitive.

If you believe that this is the case for this document, please contact [UBIRA@lists.bham.ac.uk](mailto:UBIRA@lists.bham.ac.uk) providing details and we will remove access to the work immediately and investigate.

# Rewritable Three-Dimensional Holographic Data Storage *via* Optical Forces

*Ali K. Yetisen,<sup>†, ‡,\*</sup> Yunuen Montelongo,<sup>§,\*</sup> and Haider Butt<sup>⊥</sup>*

<sup>†</sup> Harvard Medical School and Wellman Center for Photomedicine, Massachusetts General Hospital, 65 Landsdowne Street, Cambridge, Massachusetts 02139, USA

<sup>‡</sup> Harvard-MIT Division of Health Sciences and Technology, Massachusetts Institute of Technology, Cambridge, Massachusetts 02139, USA

<sup>§</sup> Department of Chemistry, Imperial College London, South Kensington Campus, London SW7 2AZ, UK

<sup>⊥</sup> Nanotechnology Laboratory, School of Engineering Sciences, University of Birmingham, Birmingham B15 2TT, UK

\* These authors contributed equally.

KEYWORDS: Photonics, Nanotechnology, Holography, Optical Tweezers, Nanoparticles, Gratings

## ABSTRACT

The development of nanostructures that can be reversibly arranged and assembled into 3D patterns may enable optical tunability. However, current dynamic recording materials such as photorefractive polymers cannot be used to store information permanently while also retaining configurability. Here, we describe the synthesis and optimization of a silver nanoparticle doped poly(2-hydroxyethyl methacrylate-*co*-methacrylic acid) recording medium for reversibly recording of 3D holograms. We theoretically and experimentally demonstrate organizing nanoparticles into 3D assemblies in the recording medium using optical forces produced by the gradients of the standing waves. The nanoparticles in the recording medium are organized by multiple nanosecond laser pulses to produce reconfigurable slanted multilayer structures. We demonstrate the capability of producing rewritable optical elements such as multilayer Bragg diffraction gratings, 1D photonic crystals and 3D multiplexed optical gratings. We also show that 3D virtual holograms can be reversibly recorded. This recording strategy may have applications in reconfigurable optical elements, data storage devices, and dynamic holographic displays.

Holography enables reconstruction of the images of the objects with intensity and wavefront information for application in imaging, data storage, and biosensors.<sup>1</sup> The storage of large amounts of digital information is a major problem for the technology industry; however, the production of a volumetric reconfigurable pattern over large numbers of writing and erasing cycles remains a challenge.<sup>2</sup> Optical forces can trap and manipulate dielectric and metal NPs with the so-called “optical tweezer” effect.<sup>3</sup> This phenomenon is enhanced when the NP has a size of the order of the electromagnetic wavelength.<sup>4</sup> Recently, this effect has been used to manipulate NPs with the interference patterns of laser beams.<sup>5</sup> This optical effect can be expanded to the holographic interference in volumetric media, which may allow the manipulation of NPs in 3D space. For example, nanosecond laser pulses was also utilized to construct multilayer diffraction gratings in functionalized hydrogel films for sensing applications.<sup>6</sup> The radiation pressure occurs due to the transfer of momentum from the scattering of incident photons. In general, the force exerted to the NP has two components: the scattering force and the gradient force.<sup>7</sup> In the case of two counter propagating beams, the scattering force vanishes and only the gradient force takes place. The gradient force originates from the anisotropic scattering of photons and it has a well-defined direction. Depending on the properties of the NP and the surrounding medium, the radiation pressure can be positive or negative.<sup>8</sup> A gradient force in the negative regime moves NPs toward regions of minimum intensity (nodes) in the standing wave.

A monomer solution consisting of hydroxyethyl methacrylate (HEMA) and crosslinker ethylene dimethacrylate (EDMA), and methacrylic acid (MAA) was prepared. A ~10  $\mu\text{m}$  thick poly(2-hydroxyethyl methacrylate-*co*-methacrylic acid) (p(HEMA-*co*-MAA)) film was coated over a silanized glass slide by free-radical polymerization. Silver nitrate ( $\text{AgNO}_3$ ) solution was

used as the ion source to create NPs (Fig. 1a). This solution was diffused into the polymer matrix and lithium bromide (LiBr) was used to convert the  $\text{Ag}^+$  ions to silver bromide (AgBr) nanocrystals (NCs) (Fig. 1b). This step is required to control the NP size distribution in the p(HEMA-co-MAA) matrix. AgBr NCs are light-sensitive; hence, they were exposed to broadband light to decrease their sensitivity to light (Fig. 1c). A photographic developer (JD-4) was used to reduce the AgBr NCs to silver metal ( $\text{Ag}^0$ ) NPs (~50-100 nm) in the p(HEMA-co-MAA) matrix (Fig. 1d). The developer's action was stopped by decreasing pH of the system below 3.0 (Fig. 1e). The unreacted AgBr NCs were extracted from p(HEMA-co-MAA) matrix by a thiosulfate treatment (Fig. 1f). The resulting matrix was immediately ready to be used as the recording medium (Fig. 1g). Figure 1h shows a scanning electron microscope image (SEM) of the p(HEMA-co-MAA) matrix cross section having  $\text{Ag}^0$  NPs ranging from 50-100 nm.

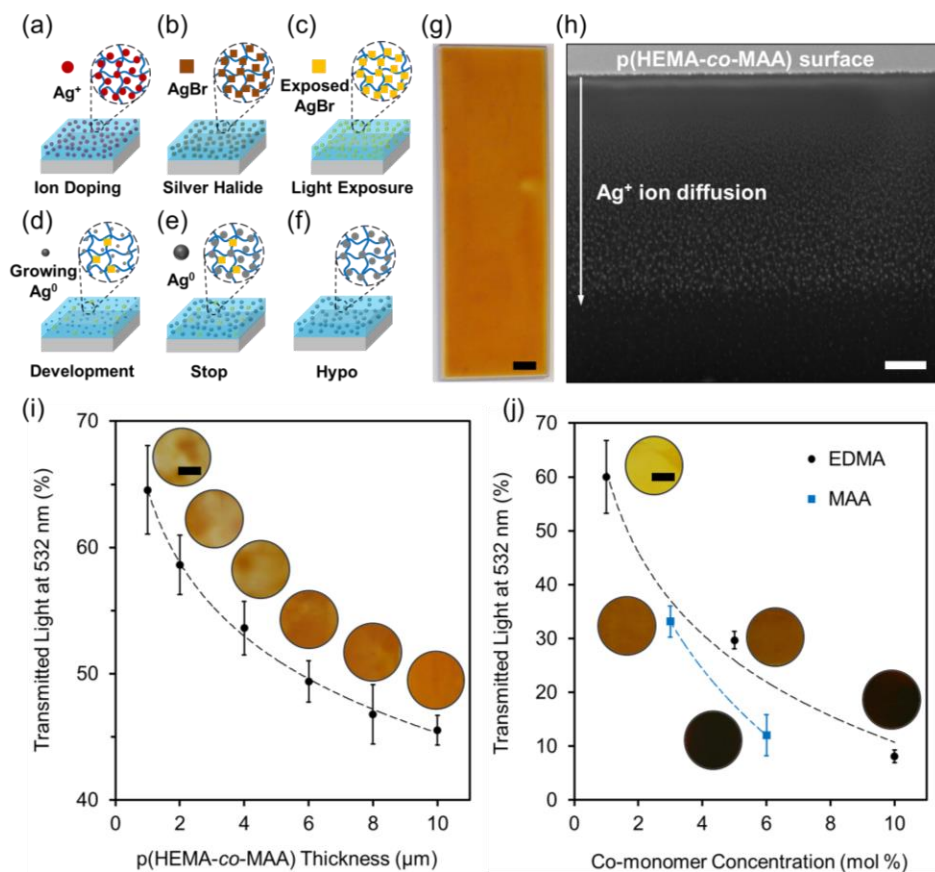


FIG. 1. Fabrication of a p(HEMA-*co*-MAA) recording medium for reconfigurable holography. (a-f) Formation of NPs in the medium. (g) Fabricated recording medium ( $t \approx 10 \mu\text{m}$ ). Scale bar = 5 mm. (h) SEM image of the recording medium cross-section. Scale bar = 1  $\mu\text{m}$ . (i) The effect of variation in thickness on light transmission through the recording medium, (j) EDMA and MAA concentrations on light transmission through the medium and  $\text{Ag}^0$  NP density. Scale bar = 5 mm.

As the thickness of matrix was increased from 1  $\mu\text{m}$  to 10  $\mu\text{m}$ , the transmitted light intensity ( $\lambda = 532 \text{ nm}$ ) through the recording medium decreased from 64% to 46% (Fig. 1i). The concentration of the EDMA was also important in retaining  $\text{Ag}^0$  NPs within the recording medium. When the concentration of EDMA was increased from 1 to 10 mol%, the transmitted light intensity through the p(HEMA-*co*-MAA) matrix decreased from 60% to 9%, corresponding to  $\text{Ag}^0$  NP density (1.3 vol%) decrease of 28 vol% (Fig. 1j). As the concentration of MAA was increased from 3 to 6 mol%, the transmitted light intensity through the matrix decreased from 33% to 12%, corresponding to  $\text{Ag}^0$  NP density increase of 25 vol% (Fig. 1j). The optimized recording medium had 2.5 mol% EDMA and 6 mol% MAA to achieve  $\sim 50\%$  light transmission and retain 1 vol%  $\text{Ag}^0$  NPs. Supplemental Material provides a protocol for the fabrication of the recording medium.<sup>9</sup>

A Nd:YAG laser (5 ns, 532 nm, 350 mJ) was set to function in Denisyuk reflection mode.<sup>10</sup> The laser beam reflected from dielectric mirrors was expanded ( $\sim 1 \text{ cm}$ ) and directed to the p(HEMA-*co*-MAA) matrix (Fig. 2a). This sample was tilted with angle  $\theta$  from the surface plane of a plane mirror. The reference beam propagated through the matrix and reflected back from the mirror (Fig. 2b). The object beam interfered with the reference beam. This process created high

intensity (antinodes) and low intensity (nodes) regions within the matrix to organize  $\text{Ag}^0$  NPs. The combination of the reference pulse and the object pulse forms a multilayer field that allows for recording the hologram. Photoinduced ablation of nanoparticles (NPs) took place during the first recording step. The reduction of  $\text{Ag}^+$  ions creates  $\text{Ag}^0$  NPs with diameters ranging from 50-100 nm. However, the first laser exposure of light attenuated the  $\text{Ag}^0$  NPs to 10-30 nm as the laser light was absorbed by the  $\text{Ag}^0$  NPs. However, no ablation takes place below this  $\text{Ag}^0$  NP diameter threshold.

The respective intensities and phases of individual plane waves were calculated. Figure 2c shows normalized field intensity patterns of a medium (50% transmission) at tilt angles ( $\theta$ ) ranging from  $0^\circ$  to  $25^\circ$ , where the reference beam is propagated from the top. The green regions in Fig. 2c show the constructive interference regions while the black regions represent destructive interference. The periodicity of the standing wave was approximately half of the laser light wavelength ( $\sim 266$  nm), and the intensity of this multilayer pattern decreased as the tilt angle increased from  $0^\circ$  to  $25^\circ$ . Additionally, the superposition of waves at different tilt angles ( $5^\circ$ - $20^\circ$ ) showed unique patterns in which the properties of multiple waves coincided.

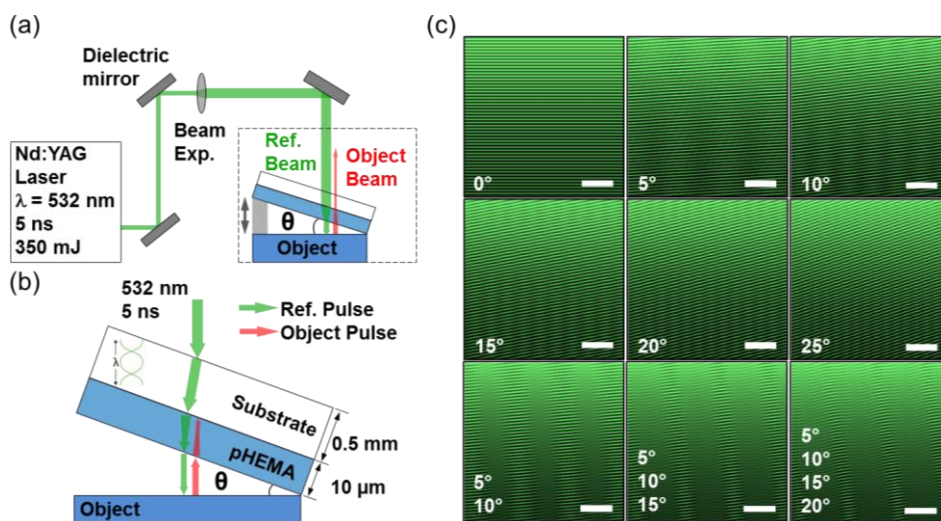


FIG. 2. Fabrication of the multilayer gratings. (a) Laser setup in Denisyuk reflection mode. (b) Formation of an interference pattern within p(HEMA-*co*-MAA) matrix. (c) Interference pattern fields at different tilt angles. Scale bars = 1  $\mu\text{m}$ .

Finite element simulations were performed to analyze the optical properties of the multilayer gratings. COMSOL Multiphysics was used to simulate the light diffraction from the photonic structures.<sup>11</sup> The geometry mesh had 2 nm resolution, where the computation was performed *via* a parametric sweep. Simulated nanostructures consisted of periodic multilayers of Ag NPs within a hydrogel matrix. A MATLAB code was utilized to generate normal random distribution of Ag<sup>0</sup> NPs (10-50 nm,  $\sigma=10$  nm) within the stacks, where the mean positions of the layers were set to lattice constants. The diffraction simulation parameters were extracted from the interference patterns modeled in Fig. 2c, where the lattice constant was  $\sim 175$  nm and the effective refractive index of the medium was 1.43. The refractive index of the domains containing Ag<sup>0</sup> NPs were set to the electrical conductivity of silver ( $61.6 \text{ mS m}^{-1}$ ). Each stack contained  $\sim 60$  Ag<sup>0</sup> NPs within 20 layers.

To simulate the grating formation in the recording medium, randomly distributed Ag<sup>0</sup> NPs were modeled over  $2 \times 2 \mu\text{m}^2$  using a MATLAB code. The displacement of NPs in each pulse was proportional to their location in the wave:  $\Delta \mathbf{x} \propto \sin(\mathbf{K} \cdot \mathbf{x})$ , where  $\mathbf{x}$  was the NP position and  $\mathbf{K}$  was the wave vector. The constant of proportionality was inferred experimentally. In each simulation, the direction of  $\mathbf{K}$  was changed to simulate the exposure angle. The refractive index of the polymer was defined as 1.37 (from the refractometer measurements). We approximated the imaginary part of the refractive index by measuring the absorption of the recording medium. We measured a light decay of 80% after crossing a thickness of 10  $\mu\text{m}$  with a 532 nm laser. The imaginary part of the refractive index was  $0.4542 i$ . The mean radii of the nanoparticles were set

within the range of 10-30 nm. The number of Ag<sup>0</sup> NPs was 18 per each stack with 11 stacks in total. The exposure wavelength was defined as 532 nm and the multilayer exposure field was simulated. Figure 3a shows the application of simulated field to a randomized medium containing Ag<sup>0</sup> NPs at different angles from the surface plane of the medium to create form multilayer diffraction gratings. Figure 3b shows the simulated optical diffraction through slanted holographic gratings recorded from 5° to 20° with respect to the surface plane of the matrix. To visualize the reflected light in the far field, the hologram was confined in a hemispherical computational domain. The diffraction spectra showed peak reflectivity at ~530 nm, which was consistent with the lattice spacing (~175 nm) of the grating. The holograms recorded at 5°, 10°, 15°, 20° showed diffraction peaks at 13°, 30°, 48°, and 65°, respectively (Fig. 3c). The diffraction peak intensities decreased 33%, 66%, 85% as the recording tilt angles was increased from 5° to 10°, 15°, and 20°, respectively.

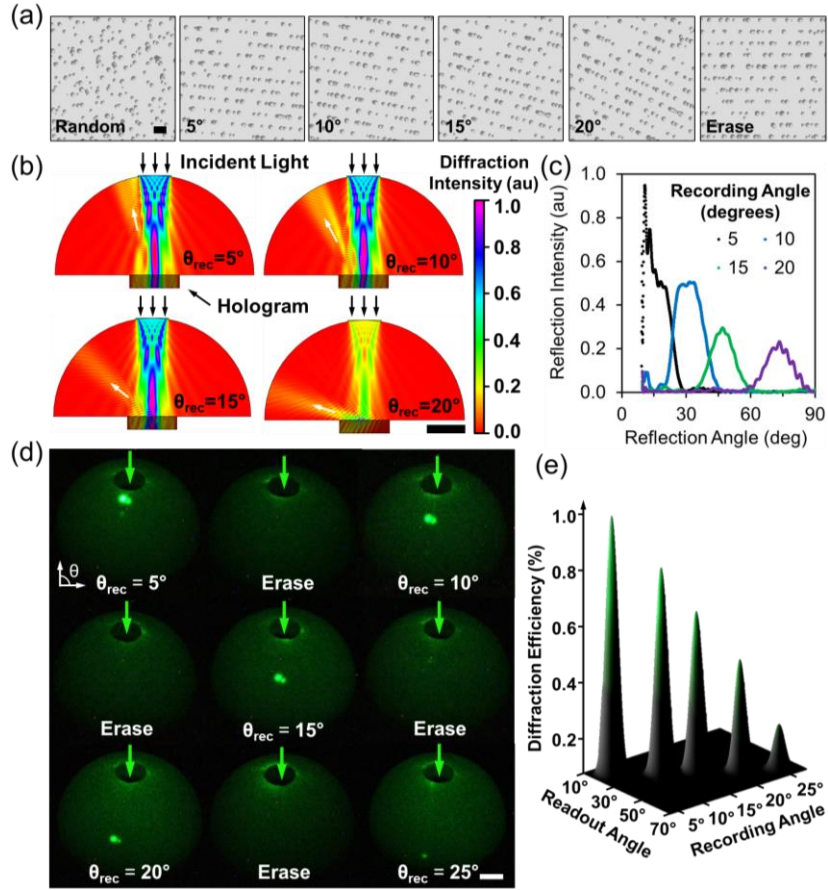


FIG. 3. Reversible holographic data storage. (a) Simulated organization of  $\text{Ag}^0$  NPs within the recording medium at different field exposures. Scale bar = 200 nm. (b) Finite element simulations of holograms shown in a semi-transparent hemisphere. Scale bar = 20  $\mu\text{m}$ . (c) Simulated optical diffraction spectra. (d) Demonstration of recording reversibility. The incident light was propagated from top. Scale bar = 1 cm. (e) Angle-resolved measurements of holograms.

To obtain the reading angle produced by a volume diffraction grating embedded in a medium with refractive index  $n$ , Bragg's law should be satisfied:

$$d \sin(\theta'_{read}) = \lambda_{eff} \quad (1)$$

where  $d$  is the oscillation distance of the slanted structure,  $\theta'_{read}$  is the reading angle in the recording medium, and  $\lambda_{eff}$  is the effective wavelength ( $\lambda/n$ ). The effective distance  $d$  is produced due to the tilt angle of the volume grating originating from the standing wave and is found with a trigonometric relation:

$$2 \sin(\theta_{record}) = \frac{\lambda_{eff}}{d} \quad (2)$$

where  $\theta_{record}$  is the tilt angle of the grating which is the same as the recording angle of the sample. The angle inside the recording medium is:

$$\sin(\theta'_{read}) = 2 \sin(\theta_{record}) \quad (3)$$

However, the reading angle ( $\theta'_{read}$ ) changes from the recording medium to air. Therefore, the reading angle in air  $\theta_{read}$  follows Snell's law:

$$n \sin(\theta'_{read}) = \sin(\theta_{read}) \quad (4)$$

Hence, the relation between the writing angle and the recording angle is:

$$\theta_{read} = \sin^{-1}(2n \sin \theta_{record}) \quad (5)$$

To demonstrate the capability of moving NPs within the medium reversibly, the holograms were recorded at 5°, 10°, 15°, 20°, and 25° tilt angles with intermediate erasing steps (recorded at 0°). Figure 3d shows the first order diffracted light over a semi-transparent hemisphere as the holograms were normally illuminated with 532 nm laser light. The modulation was mostly in phase rather than in amplitude since the effective refractive index change when NPs migrate. The measured index of refraction of the recording medium without NPs was 1.37 and with NPs was

1.43. The increase in the effective refractive index of the recording medium is due to the reduction of  $\text{Ag}^+$  ions to  $\text{Ag}^0$  NPs by the photographic developer. This difference in refractive index was significant enough to produce a considerable phase modulation. The change in both the real and the imaginary parts of the refractive index will induce diffraction. A periodic variation of amplitude, or phase, or both will create diffraction.<sup>12</sup> Furthermore, this phenomenon is observed in both transmission and reflection modes. The period of the oscillation was extracted with a trigonometrical identity with the recording angle.

The process of hologram recording was fully reversible, demonstrated by erasing the hologram at  $0^\circ$  tilt angle from the surface plane of the mirror to align the first order diffracted light with specular reflection. In this holographic erasure process, the laser pulse is incident to the surface plane of the recording medium. Hence, the formed Ag NPs are organized in multilayer that runs parallel to the substrate. The distance that nanoparticles move within the recording medium depends on the number and energy of the laser pulses. We recorded and erased these structures over 30-40 cycles without significant change in the diffraction efficiency. As the recording angle was increased, the first order diffracted light from the normal shifted from  $15^\circ$  to  $66^\circ$  (Fig. 3e). The decrease in the diffraction intensity with increasing diffraction angle can be attributed to the interference of the transmission grating.

Figure 4a illustrates simulated geometry of superimposed holographic gratings. Figure 4b shows simulated optical diffraction of superposed holograms recorded at  $5^\circ$ ,  $10^\circ$ , and  $5^\circ$ ,  $10^\circ$ ,  $15^\circ$  with respect to the surface plane of the matrix. The holograms superposed at  $5^\circ$  and  $10^\circ$  had simulated diffraction peaks at  $21^\circ$  and  $33^\circ$ , respectively (Fig. 4c). When three holograms were superposed at  $5^\circ$ ,  $10^\circ$ , and  $15^\circ$  the diffraction peaks were at  $22^\circ$ ,  $38^\circ$ , and  $50^\circ$  (Fig. 4c). The

average intensity of the simulated diffraction peaks of these three diffraction spots were  $\sim 60\%$  lower than those of the holograms superposed at  $5^\circ$  and  $10^\circ$ .

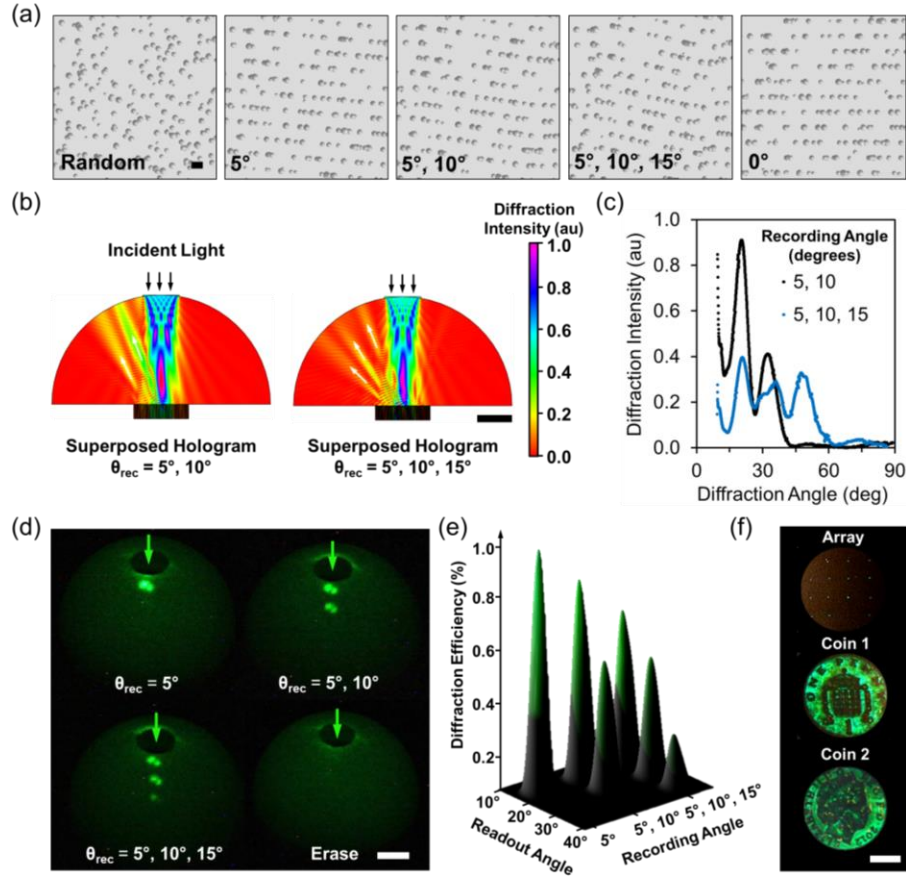


FIG. 4. Reversible recording of superposed holographic data. (a) Simulated organization of  $\text{Ag}^0$  NPs. Scale bar = 200 nm. (b) Finite element simulations.  $\theta_{\text{rec}}$  = recording tilt angle. Scale bar = 20  $\mu\text{m}$ . (c) Simulated diffraction spectra. (d) Demonstration of superposed gratings on subsequent recording steps. Scale bar = 1 cm. (e) Angle-resolved measurements. (f) Rewritable holographic array and 3D virtual images of coins. Scale bar = 5 mm.

To superpose the holograms, the first hologram was recorded at  $5^\circ$  from the surface plane of the mirror, and subsequently the second and third holograms were recorded at  $10^\circ$  and  $15^\circ$  within the same p(HEMA-*co*-MAA) matrix. In this procedure, the hologram was not erased between the recording steps. This process allowed superposing holographic gratings at  $5^\circ$ ,  $10^\circ$ , and  $15^\circ$  tilt

angles iteratively (Fig. 4d). The superposed hologram diffracts light at distinct angles. Similarly, angle-resolved measurements of the superposed holograms at 5°, 10°, and 15° tilt angles showed diffraction at 15°, 25°, and 40°, respectively (Fig. 4e). The intensity of the diffracted spot at 40° was lower than the spots at 15° and 25°. Figure 3f shows a holographic array (4×4) and virtual holograms recorded using coins, followed by an erasing process. During the experiments, no fatigue was observed in the p(HEMA-*co*-MAA) matrix. The recorded holograms showed full parallax and efficiently diffracted the incident light. The described simulation model and fabrication strategy to reversibly record holograms may find applications in dynamic displays, printable optical devices, and security.

## AUTHOR INFORMATION

### Corresponding Author

\* e-mail: ayetisen@mgh.harvard.edu

## REFERENCES

- <sup>1</sup> M. Haw, *Nature* **422** (6932), 556 (2003); D. E. Smalley, Q. Y. Smithwick, V. M. Bove, Jr., J. Barabas, and S. Jolly, *Nature* **498** (7454), 313 (2013); N. M. Farandos, A. K. Yetisen, M. J. Monteiro, C. R. Lowe, and S. H. Yun, *Adv Healthc Mater* **4** (6), 792 (2015); A.K. Yetisen, H. Butt, and S. H. Yun, *ACS Sensors* **1** (5), 493 (2016); A. K. Yetisen, Y. Montelongo, M. M. Qasim, H. Butt, T. D. Wilkinson, M. J. Monteiro, and S. H. Yun, *Anal. Chem.* **87** (10), 5101 (2015); AK Yetisen, MM Qasim, S Nosheen, TD Wilkinson, and CR Lowe, *J. Mater. Chem. C* **2** (18), 3569 (2014); A. K. Yetisen, Y. Montelongo, F. da Cruz Vasconcellos, J. L. Martinez-Hurtado, S. Neupane, H. Butt, M. M. Qasim, J. Blyth, K. Burling, J. B. Carmody, M. Evans, T. D. Wilkinson, L. T. Kubota, M. J. Monteiro, and C. R. Lowe, *Nano Lett* **14** (6), 3587 (2014); A. K. Yetisen, H. Butt, F.C. Vasconcellos, Y. Montelongo, C.A.B. Davidson, J. Blyth, L. Chan, J. B. Carmody, S. Vignolini, U. Steiner, J.J. Baumberg, T.D. Wilkinson, and C.R. Lowe, *Adv. Opt. Mater.* **2** (3), 250 (2014); A. K. Yetisen, H. Butt, T. Mikulchyk, R. Ahmed, Y. Montelongo, M. Humar, N. Jiang, S. Martin, I. Naydenova, and S. H. Yun, *Adv. Opt. Mater.* DOI: 10.1002/adom.201600162 (2016); A. K. Yetisen, I. Naydenova, F.C. Vasconcellos, J. Blyth, and C.R. Lowe, *Chem. Rev.* **114** (20), 10654 (2014).

- <sup>2</sup> L. Hesselink, S. S. Orlov, A. Liu, A. Akella, D. Lande, and R. R. Neurgaonkar, *Science* **282** (5391), 1089 (1998).
- <sup>3</sup> O. M. Maragò, P. H Jones, P. G Gucciardi, G. Volpe, and A. C. Ferrari, *Nat. Nanotechnol.* **8** (11), 807 (2013).
- <sup>4</sup> Y. Montelongo, A.K. Yetisen, H. Butt, and S.H. Yun, *Nat. Commun.* **7**, 12002 (2016).
- <sup>5</sup> A. K. Yetisen, Y. Montelongo, N. M. Farandos, I. Naydenova, C. R. Lowe, and S. H. Yun, *Appl. Phys. Lett.* **105** (26), 261106 (2014).
- <sup>6</sup> M. Zawadzka, T. Mikulchyk, D. Cody, S. Martin, A.K. Yetisen, J. L. Martinez-Hurtado, H. Butt, E. Mihaylova, H. Awala, S. Mintova, S. H. Yun, and I. Naydenova, in *Photonic Materials for Sensing, Biosensing and Display Devices*, edited by M.J. Serpe, Y. Kang, and Q.M. Zhang (Springer, Switzerland, 2016), pp. 315.
- <sup>7</sup> K. C. Neuman and S. M. Block, *Rev. Sci. Instrum.* **75** (9), 2787 (2004).
- <sup>8</sup> M. Šiler, L. Chvátal, and P. Zemánek, *J. Quant. Spectrosc. Radiat. Transf.* **126**, 84 (2013).
- <sup>9</sup> See supplemental material at [URL will be inserted by AIP] for materials, instruments, synthesis of *p*(HEMA-co-MAA) matrix, and fabrication of the recording medium. .
- <sup>10</sup> S. A. Benton and V. M. Bove, in *Holographic Imaging* (John Wiley & Sons, Inc., 2007), pp. 173; Q. Zhao, A. K. Yetisen, C. J. Anthony, W. R. Fowler, S. H. Yun, and H. Butt, *Appl. Phys. Lett.* **107** (4), 041115 (2015); F. C. Vasconcellos, A. K. Yetisen, Y. Montelongo, H. Butt, A. Grigore, C.A.B. Davidson, Jeff Blyth, M. J. Monteiro, T. D. Wilkinson, and C. R. Lowe, *ACS Photonics* **1** (6), 489 (2014); Q. Zhao, A. K. Yetisen, A. Sabouri, S. H. Yun, and H. Butt, *ACS Nano* **9** (9), 9062 (2015).
- <sup>11</sup> A. Breuer-Weil, N. N. Almasoud, B. Abbasi, A. K. Yetisen, S. H. Yun, and H. Butt, *Nanoscale Res Lett* **11** (1), 157 (2016); C. P. Tsangarides, A. K. Yetisen, F. C. Vasconcellos, Y. Montelongo, M. M. Qasim, T. D. Wilkinson, C. R. Lowe, and H. Butt, *RSC Adv.* **4** (21), 10454 (2014).
- <sup>12</sup> M. Born, E. Wolf, and A.B. Bhatia, *Principles of Optics: Electromagnetic Theory of Propagation, Interference and Diffraction of Light*, 7 ed. (Cambridge University Press, United Kingdom, 1999).